Chapter 6

Comparision with Theoretical Predictions

6.1 Experiment Evidence for Shell Effects

One of the most obvious indications for the existence of the shell structure is obtained by the investigation of the neutron (proton) separation energy $S_{2n}(S_{2p})$. These nuclear observables are independent of the strong pairing effect between nucleons and are presented for the Sn (Z=50) nuclei for different neutron numbers N in the interval 52≤N≤84 in fig. 6.1. At N=82, a clear discontinuity shows up in S_{2n}. The extra stability at the neutron number 2, 8, 20, 28, 50, 82 and 126 is very clearly present in investigations over a much larger mass region.

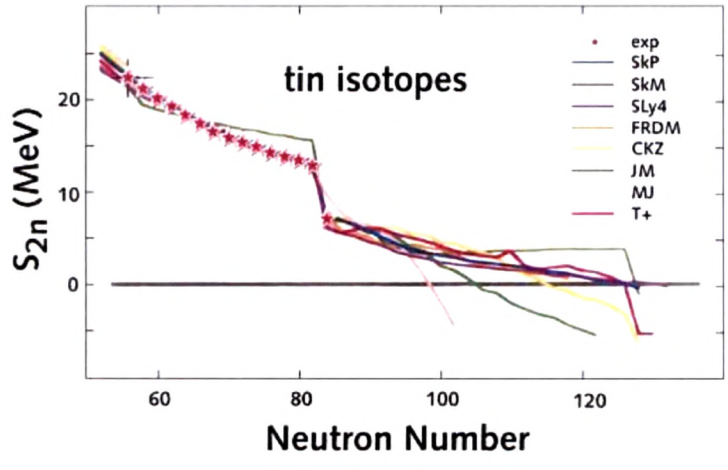

Figure 6.1: Two-neutron separation energy S_{2n} for the tin isotopes as a function of the neutron number.

A number of other indicators are obtained by studying the Z, N variations of various nuclear observables, e.g. excitation energy $E_{2_1^+}$ of the first excited state in all even-even nuclei (see fig. 1.1).

6.2 The Average Potential of the Nucleus

In the conventional theory of the nuclear structure at low energies the nucleus is treated as a quantum-mechanical many-body problem of Fermions interacting by a non-relativistic two-body interaction (see for instance [39, 40]). The starting point is the nuclear A-body Hamiltonian

$$H = \sum_{i=1}^{A} \frac{\vec{p_i}^2}{2 \cdot m_i} + \sum_{i<j}^{A} V(\vec{r_i}, \vec{r_j}) \tag{6.1}$$

With the assumption that nucleons mainly move independently from each other in an average field with a large mean-free path, the above equation reduces to a much simpler equation

$$H_0 + H_{res} = \left[\sum_{i=1}^{A} \frac{\vec{p_i}^2}{2 \cdot m_i} + U(\vec{r_i}) \right] + \left[- \sum_{i=1}^{A} U(\vec{r_i}) + \sum_{i<j}^{A} V(\vec{r_i}, \vec{r_j}) \right] \tag{6.2}$$

In the following the residual interaction H_{res} is neglected. If one considers the spin-orbit coupling, the single-particle spectra are obtained which yield the correct 'magic' nuclear numbers. Besides the correct reproduction of global properties of the nucleus, a microscopic calculation should also aim at a correct description of finer details, i.e. local excitations in the nucleus. This is a highly ambitious task since the typical energy scales (binding energy $E_0 \sim 10^3$MeV, excitation energies E_x ~1-2MeV) differ by three orders of magnitude. The starting point should be a realistic interaction, i.e. a potential $V(\vec{r_i}, \vec{r_j})$ which reproduces the nucleon-nucleon scattering properties in the energy region 0-500MeV. Typical radial shapes for $V(\vec{r_i}, \vec{r_j})$ are Yukawa shapes [41]

$$V(r) = \frac{e^{-\mu \cdot r}}{\mu \cdot r} \tag{6.3}$$

with $r \equiv | \vec{r_1} - \vec{r_2} |$.
One of the problems related to the study of nuclear structure at low excitation energy is the choice of the model space to be used. Including explicit correlations between nucleons, the model space expands quickly with the number of particles. Modern large-scale shell-model configurations try to treat many or all of the possible ways in which nucleons can be distributed over the available single-particle orbits that are important in a particular mass region. It is clear that nuclei in the mid-shell region will obtain a very large model space and extensive numerical computations will be needed. The increase in computing facilities has made the implementation of large model spaces and configuration mixing possible. In the present case a ^{90}Zr or ^{100}Sn core was used which requires an effective charge for the valence

particles.

6.2.1 The Electric Quadrupole Moment and Effective Charges

The non-spherical distribution of the charges in a nucleus gives rise to a quadrupole moment. The classical definition of the charge quadrupole moment operator in a Cartesian axis system is given [42] by:

$$Q_z = \sum_{i=1}^{A} e_i \cdot (3z_i^2 - r_i^2) \tag{6.4}$$

with e_i being the charge of the respective nucleon and (x_i,y_i,z_i) its coordinates. In a spherical tensor basis the z-component of the quadrupole operator is more easily expressed as the zero order tensor component of rank 2 tensor:

$$Q_{20} = Q_z = \sum_{i=1}^{A} e_i \cdot r_i^2 \cdot Y_{20}(\theta_i, \phi_i) \cdot \sqrt{\frac{16\pi}{5}} \tag{6.5}$$

The nucleus is a quantum mechanical system that is described by a nuclear wave function, characterized by a nuclear spin I. In experiments we observe the spectroscopic quadrupole moment, which is the expectation value of the quadrupole operator, defined as

$$Q(I) = \langle IM||\hat{Q}_z||IM\rangle_{M=I} \tag{6.6}$$

or with spherical tensor notation

$$Q(I) = \langle IM||\hat{Q}_{20}||IM\rangle_{M=I} \tag{6.7}$$

In the shell model, the nuclei are described by a nuclear mean field (core) in which some individual valence nucleons move and interact with each other through a residual interaction. For calculating the spectroscopic quadrupole moment, the sum over all nucleons in expression (Eq. 6.5 and Eq. 6.7) is reduced to the sum over the valence particles. In the extreme single particle shell model the quadrupole moment of an odd-proton (or an odd-neutron) nucleus with spin I is determined by the single particle moment of the unpaired proton (or neutron) in the orbital j. If I=j, then quadrupole moment is given by the single-particle moment [43]

$$Q_{sp} = -e_j \cdot \frac{2j-1}{2j+2} \cdot \langle r_j^2 \rangle \tag{6.8}$$

Here e_j is the charge of the nucleon in orbital j and $\langle r_j^2 \rangle$ is the mean square radius of the nucleon in that orbital. Note that free neutrons have no charge, $e_\nu = 0$, and therefore do not induce a single-quadrupole moment. Free protons with $e_\pi = +1$ induce a negative quadrupole moment.

However, valence nucleons in a nucleus interact with the nucleons of the core and can polarize the core, which is reflected by giving neutrons as well as protons an effective charge.

This is illustrated in fig. 6.2. The effective charges are model dependent: if a smaller model space is taken for the valence nucleons, the effective charge needed to reproduce the experimental quadrupole moments deviate more from the nucleon charges. However, for a large enough model space, the effective charges are found to be constant in a broad region of nuclei and closer to the free charges of the nucleons. Effective charges have been determined in several regions of the nuclear chart by comparing experimental quadrupole moments of nuclei, whose proton or neutron number deviates from doubly-magic by 1. Typical values vary from $e_\pi^{eff} \approx 1.3$e, $e_\nu^{eff} \approx 0.3$e in light nuclei [44] to $e_\pi^{eff} \approx 1.6$e, $e_\nu^{eff} \approx 0.95$e in the lead region [45].

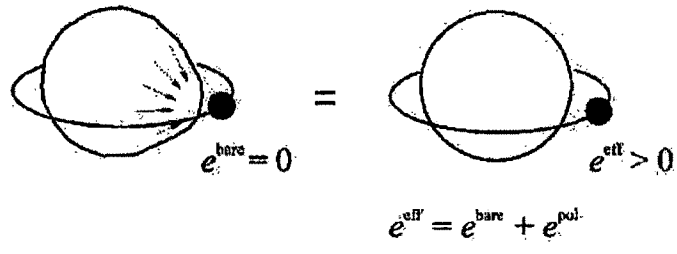

Figure 6.2: Effective charge for a neutron induced by the attractive strong interaction between single nucleon and the core.

Nuclei near shell closures are considered to be spherical which are described by a wave function of individual nucleons moving in a spherical potential. Therefore, the core does not contribute to the nuclear quadrupole moment (single particle Q-moments are <0.5eb). Due to particle-core interactions, the valence nucleon can polarize the core. Because the nuclear energy is minimized if the overlap of the core nucleons with the valence particle (or hole) is maximal, a particle (respective hole) will polarize the core towards an oblate (respectively prolate) deformation, as demonstrated in fig.6.3.

A change of the quadrupole moment as a function of N or Z can be either a signature for a change in the core polarization or, if the change is drastic, an indication for an onset of a static nuclear deformation. For example, the systematic increase of quadrupole moments with decreasing neutron number in neutron-deficient Po isotopes (see fig.6.4) has been explained by an increase of the quadrupole-quadrupole interaction between the proton particles and the increasing amount of neutron holes [46, 47].

6.2.2 Comparision with Large-Scale-Shell-Model Calculations

In the first set of large-scale shell-model (LSSM) calculations (for details see [4]) performed by the Oslo group for all tin isotopes $^{102-130}$Sn, the CD-Bonn potential for the bare nucleon-nucleon interaction [48] was used. Two sets of closed shell core were chosen for these calculations, ^{100}Sn and ^{132}Sn. In the present discussion we focus on the results obtained with

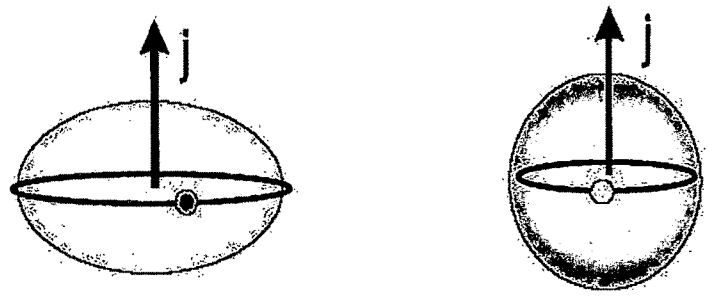

Figure 6.3: Graphical representation of a particle in an orbital j, polarizing the core towards oblate deformation with a negative quadrupole moment (left), and a hole in an orbital giving rise to a prolate core polarization (right).

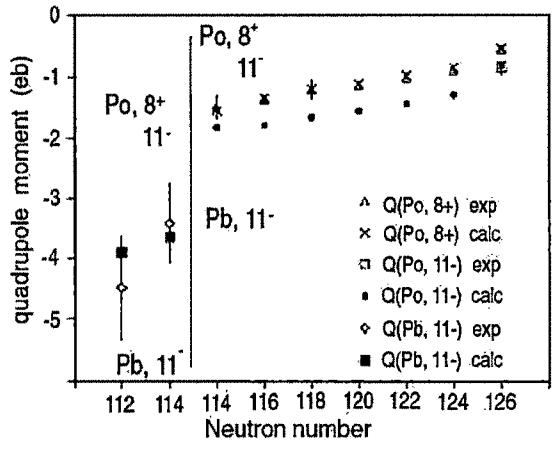

Figure 6.4: The increase in the absolute value of the quadrupole moments of isomers in the Pb region has been understood as due to a coupling of the valence particles with the quadrupole excitations of the underlying core.

the ^{100}Sn closed-shell core. The model space for neutrons comprises in all cases of the $1d_{5/2}$, $0g_{7/2}$, $1d_{3/2}$, $2s_{1/2}$ and $0h_{11/2}$ orbitals. A harmonic-oscillator basis was chosen for the single-particle wave functions, with an oscillatory energy $\hbar\omega = 45 \cdot A^{-1/3} - 25 \cdot A^{-2/3} = 8.5$MeV. The single-particle energies of the chosen model space orbits are set, relative to the $1d_{5/2}$ orbital ($\epsilon_{1d5/2}$=0.0MeV), as follows: $\epsilon_{0g7/2}$=0.08MeV, $\epsilon_{1d3/2}$=1.66MeV, $\epsilon_{2s1/2}$=1.55MeV, and $\epsilon_{0h11/2}$=3.55MeV. The neutron effective charge was set to 1.0e. The results of the calculations for the energies of the 2_1^+ excites states and the B(E2;$0^+_{g.s} \rightarrow 2_1^+$) values are presented in columns 3 and 5 of tab. 6.1 together with experimental data.

To shed more light on the role of core polarization effects, a second set of LSSM calculations includes protons in the $0g_{9/2}$, $0g_{7/2}$, $1d_{5/2}$, $1d_{3/2}$ and $2s_{1/2}$ single-particle orbits as well, in addition to neutrons in the same model space as in the first set of calculations. The calculations, performed with the coupled code NATHAN [49], allowed up to 4p-4h proton core excitations. The closed-shell core is this time ^{90}Zr and the effective charges are set to 1.5e and 0.5e for protons and neutrons, respectively. In this model space the m-scheme dimension was excessively large. Because of the seniority truncation in that calculation the systematic trend in B(E2↑) values was retained. The comparision between experiment and theory shows agreement for the heavier Sn isotopes assuming a ^{100}Sn core. However, for the lighter Sn isotopes one observes an asymmetry of the B(E2↑) systematics. The experimental information

Isotope	$E(2_1^+)$ [keV]		$B(E20_{g.s}^+ \rightarrow 2_1^+)$ e^2b^2		
	Exp	SM^b	*Exp*	SM^b	SM^c
^{102}Sn	1472.0(2)	1647		0.043	0.044
^{104}Sn	1260.1(3)	1343		0.094	0.090
^{106}Sn	1207.7(5)	1231	0.209(32)	0.137	0.125
^{108}Sn	1206.1(2)	1243	0.224(16)	0.171	0.162
^{110}Sn	1211.9(2)	1259	0.226(18)	0.192	0.192
^{112}Sn	1256.9(7)	1237	0.242(8)	0.203	0.219
^{114}Sn	1299.9(7)	1208	0.232(8)	0.209	0.235
^{116}Sn	1293.6(8)	1135	0.209(6)	0.210	0.241
^{118}Sn	1229.7(2)	1068	0.209(8)	0.208	0.239
^{120}Sn	1171.3(2)	1044	0.202(4)	0.201	0.228
^{122}Sn	1140.6(3)	1076	0.192(4)	0.184	0.206
^{124}Sn	1131.7(2)	1118	0.166(4)	0.156	0.174
^{126}Sn	1141.2(2)	1214	0.10(3)	0.118	0.134
^{128}Sn	1168.8(4)	1233	0.073(6)	0.079	0.090
^{130}Sn	1121.3(5)	1191	0.023(5)	0.042	0.047

[b]LSSM in $\nu(g_{7/2}$, d, s, $h_{11/2})$ shell model space with ^{100}Sn closed-shell core and e^{ν}_{eff}=1.0e.
[c]LSSM in π(g, d, s) and $\nu(g_{7/2}$, d, s, $h_{11/2})$ shell model space with ^{90}Zr closed-shell core and the effective charge e^{π}_{eff}=1.5e and e^{ν}_{eff}=0.5e.

Table 6.1: $I^{\pi}=2^+$ energies and E2 strengths in $^{102-130}$Sn. The experimental data of the neutron-deficient isotopes are averaged values of Refs. [6, 14, 15, 16].

in the B(E2↑) systematics of the tin isotopes with the new values of ^{112}Sn and ^{114}Sn included is also presented in fig. 6.5. It is appearent that the result from ^{112}Sn is about 20% larger than the one for ^{120}Sn, in contrast to the symmetric distribution expected with respect to the midshell A=116. According to the seniority model the B(E2↑) values naturally decrease with the decreasing number of particles outside the closed core. This trend cannot be found in our data for ^{112}Sn and ^{114}Sn.

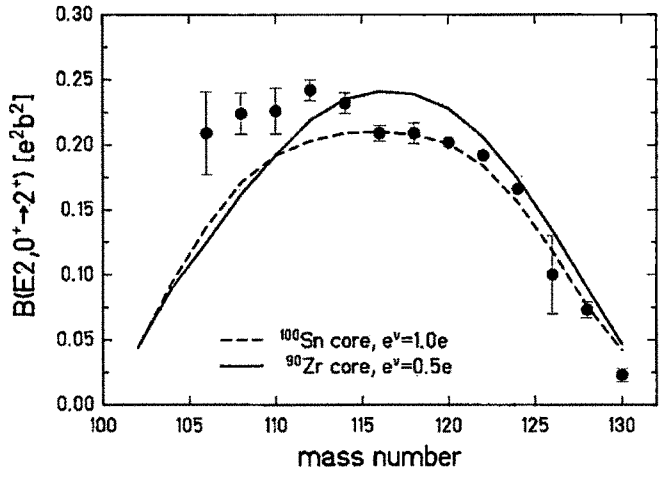

Figure 6.5: Experimental data on B(E2;$0^+_{g.s} \rightarrow 2^+_1$) values in the Sn isotope chain from the current results for ^{112,114}Sn and from [2, 6, 14, 15, 16]. The dotted and the full lines show the predictions of the large-scale shell model calculations [6] performed with a ^{100}Sn core and a ^{90}Zr core, respectively.

6.3 Relativistic Quasi-Particle Random Phase Approximation

For the study of the heavier nuclei alternative methods have been developed, usually in the form of self-consistent mean field theories. Phenomenological in nature (an effective interaction and an average potential is introduced), their success in describing bulk nuclear properties all across the nuclear chart make them a very good tool for the study of nuclear phenomena.

It is understood that the interaction $V(\vec{r_i}, \vec{r_j})$ in a nucleus has its origin in the exchange of mesons between the bare nucleons. The simplest form is the one-pion exchange potential which has the radial dependence of the Yukawa potential [41]. In eq. 6.3 the parameter $1/\mu = \hbar/m_\pi c$ denotes the Compton wavelength of the pion.

In the relativistic mean field approximation RMF [51], nucleons are described as Dirac point-like particles that interact by the exchange of different type of mesons. The attraction of nucleons is caused by the scalar meson $\sigma(I^\pi = 0^+$,T=0) field. The short repulsive interaction is connected with the exchange of vector meson $\omega(I^\pi = 1$,T=0). The isovector meson

$\rho(I^\pi = 0^-$,T=1) is also included. The electromagnetic interaction is carried by a photon field. Although nucleons in nuclei have relatively small kinetic energies as compared to the rest mass, there are reasons to study the nuclear many body problem in the relativistic framework. As a direct consequece of relativity two mean fields appear, i.e. an attractive scalar field S and a repulsive vector field V which characterise the essential features of nuclear systems, i.e. the shell structure. Their difference (V-S) determines the weak nuclear mean field in which nucleons move and their sum (V+S) the strong spin-orbit term.

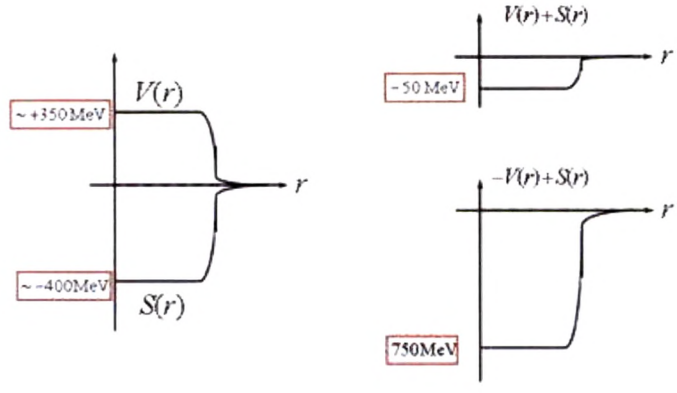

Figure 6.6: The attractive scalar field S(r) and the repulsive vector field V(r) form the weak nuclear mean field (S+V) and the strong spin-orbit term (S-V).

6.3.1 Density Functional Theory

The density functional theory is a quantum mechanical method used in many areas of physics to investigate many-body systems. For such a system the ground state expectation value for the Hamiltonian is the state energy

$$E_0 = \left\langle \Psi_0 | \hat{H} | \Psi_0 \right\rangle = \left\langle \Psi_0 | \hat{T} + \hat{U} + \hat{V} | \Psi_0 \right\rangle \tag{6.9}$$

where, in the customary decomposition of $\hat{H}$, $\hat{T}$ is the kinetic energy term, $\hat{U}$ is the term corresponding to the interaction between particles and $\hat{V}$ is an external potential. For a given wave function Ψ one can calculate the local simple particle density as

$$\rho(r) = \int d^3r_2 ... \int d^3r_N \Psi^*(r, r_2, .., r_N)\Psi(r, r_2, .., r_N) \tag{6.10}$$

The previous relation can be inverted: for a given ground state density $\rho(r)$, it is possible, in principle, to calculate the corresponding ground state wave function Ψ_0. This means that Ψ_0 is a function of $\rho(r)$, and consequently, all ground state observables are functional of

$\rho(r)$, too. Therefore, it is possible to calculate all properties of the system, in particular, its ground state energy E_0=E(ρ). By minimization of the energy functional with respect to the density one obtains the ground state energy and density of fermionic system. This gives an alternative way to describe an interacting system of fermions via its density and not via its many-body wave function. The greatest advantage of this method is that one does not have to assume an inert core and adjust effective charge parameters for protons and neutrons from nucleus to nucleus or region to region of the periodic table.

One uses a phenomenological description of the nuclear many body problem and solves it with an effective density dependent energy functional. The parameters of these functional are fitted to the experimental data of nuclear matter and of finite nuclei. The number of mesons, their quantum numbers such as spin I, Parity P and isospin T and the values of their masses and coupling constants are determined in such a way as to reproduce as well as possible the experimental data. Simplicity is an essential ingredient. One therefore tries to include only as few as mesons as possible. There are eight free parameters in the relativistic mean field model: meson masses and their coupling constants.
Various sets of interaction coupling constants - going by names such as NL1, NL-SH, and NL3 - are considered in the literature (see tab. 6.2)

	NL1	NL-SH	NL3
m [MeV]	938.0	939.0	939.0
m_σ [MeV]	492.25	526.059	508.194
m_ω [MeV]	795.359	783.0	782.501
g_σ	10.138	10.444	10.217
g_ω	13.285	12.945	12.868
g_ρ	4.976	4.383	4.474
g_2 [fm^{-1}]	-12.172	-6.9099	-10.431
g_3	-36.265	-15.8337	-28.885
K_{nm}[MeV]	211.7	355.0	271.8

Table 6.2: Relativistic mean field parameterizations NL1, NL-SH and NL3. K_{nm} corresponds to the incompressibility of the matter for each set of parameters. The mass of the ρ meson is fixed to the experiment value, m_ρ=763.0 MeV.

Relativistic Hartree-Bogoliubov (RHB) theory was successfully applied to the study of many ground state properties in nuclei throughout the periodic table. It shows a high degree of accuracy in the reproduction of experimental data: masses and radii, shape coexistence, halos, neutron and proton rich nuclei, rotational bands and nuclear magnetism, superdeformation, etc.
For the description of vibrational excited states, the standard approach is the random-phase approximation (RPA) in the doubly magic spherical nuclei and it is the quasi-particle RPA

in open-shell spherical nuclei. RING and co-workers [52, 53] have recently derived fully self-consistent relativistic RPA and QRPA equations based on the RHB mean field. For the interaction in the particle-hole channel three different density functionals were used, i.e. the standard RMF functional with non-linear meson self interaction, the RMF functional with density dependent meson-nucleon coupling constants, and the RMF functional with density dependent point couplings. The same interaction is used for the ground state and excited states calculation. The two-quasiparticle QRPA configuration space include states with both nucleons in discrete bound levels, states with one nucleon in the continuum, and also states with both nucleons in the continuum.

6.3.2 Comparision with Relativistic Quasi-Particle Random Phase Approximation

Recently [54], this approach has been applied to calculate the energies of the first excited 2^+ states and corrsponding B(E2) decay data for tin isotopes with even mass numbers A=100-134. The great advantage of the RQRPA scheme is that it is not necessary to assume an inert core and to adjust parameters of the Hamiltonian from nucleus to nucleus or region to region of the periodic table. In tab. 6.3 we compare the measured B(E2$\uparrow$) values of the Sn isotopes with the calculated data [54]. In view of there being no free adjustment of parameters or effective charges, the agreement with theoritical data is very good. The most important feature is the asymmetric behaviour of the B(E2$\uparrow$) data with respect to the midshell nucleus ^{116}Sn. Fig. 6.7 shows the comparision of the experimental B(E2$\uparrow$) values of the tin isotopes with the RQRPA calculations. It is interesting to note that the same RQRPA calculations yield quite satisfactory agreement also for the Ni and Pb isotopes [55].

Isotope	$E(2_1^+)$ [keV]		$B(E20_{g.s}^+ \rightarrow 2_1^+)$ e^2b^2	
	Exp	*RQRPA*	*Exp*	*RQRPA*
^{102}Sn	1472.0(2)	1341		0.094
^{104}Sn	1260.1(3)	1001		0.185
^{106}Sn	1207.7(5)	891	0.209(32)	0.235
^{108}Sn	1206.1(2)	940	0.224(16)	0.227
^{110}Sn	1211.9(2)	1014	0.226(18)	0.202
^{112}Sn	1256.9(7)	1112	0.242(8)	0.176
^{114}Sn	1299.9(7)	1207	0.232(8)	0.155
^{116}Sn	1293.6(8)	1236	0.209(6)	0.144
^{118}Sn	1229.7(2)	1242	0.209(8)	0.146
^{120}Sn	1171.3(2)	1269	0.202(4)	0.150
^{122}Sn	1140.6(3)	1296	0.192(4)	0.152
^{124}Sn	1131.7(2)	1340	0.166(4)	0.145
^{126}Sn	1141.2(2)	1411	0.10(3)	0.126
^{128}Sn	1168.8(4)	1537	0.073(6)	0.096
^{130}Sn	1121.3(5)	1751	0.023(5)	0.055

Table 6.3: $I^\pi=2^+$ energies and E2 strengths in $^{102-130}$Sn. The experimental data of the neutron-deficient isotopes are averaged values of Refs. [6, 14, 15, 16]

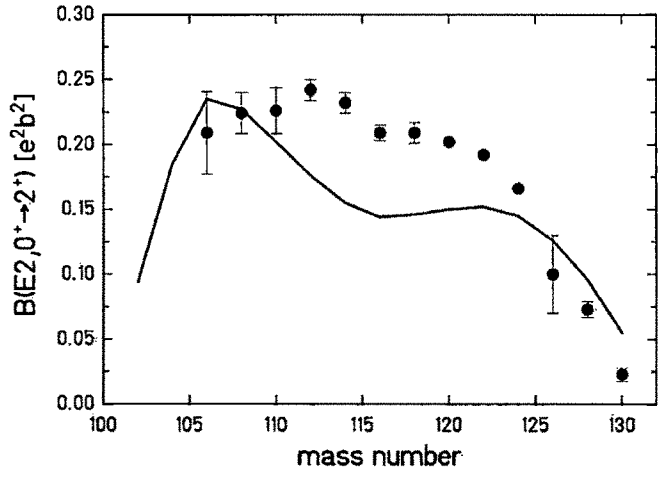

Figure 6.7: Experimental data on $B(E2;0_{g.s}^+ \rightarrow 2_1^+)$ values in the Sn isotope chain from the current results for ^{112,114}Sn and from [2, 6, 14, 15, 16]. The full line shows the predictions of the RQRPA calculations [54]